The effects of cationic impurities on the performance of proton exchange membrane water electrolyzer

Li, Na; Simon Araya, Samuel; Cui, Xiaoti; Kær, Søren Knudsen

The effects of cationic impurities on the performance of proton exchange membrane water electrolyzer

Na Li, Samuel Simon Araya [a,*], Xiaoti Cui [a], Søren Knudsen Kær [a]

[a] Aalborg University, Department of Energy Technology, Pontoppidanstræde 111, 9220 Aalborg Øst, Denmark

Abstract

This paper investigates the effects of impurities contamination on the performance of a proton exchange membrane (PEM) water electrolyzer. The impacts of Fe^{3+}, Cu^{2+} and Al^{3+} ions on the performance of single PEM water electrolysis cells are investigated by introducing $Fe_2(SO_4)_3$, $CuSO_4$, $Al_2(SO_4)_3$ solution into deionized water to prepare 5 parts per million (ppm, molar ratio) contaminated feed solution. The prepared solution was then fed to the PEM water electrolysis system to carry out the contamination test. The results show that the single cell performance experienced a dramatic decrease initially but then recovered to some degree during the Fe^{3+} ions contamination. For Cu^{2+} ions contamination, the cell ohmic resistance decreased while the charge and mass transfer resistance showed an increasing trend throughout the test period. Moreover, the Al^{3+} ions can cause a sudden cell failure when introduced into the cell.

Keywords: PEM water electrolysis, Impurity contamination, Impedance Spectroscopy, Degradation

1. Introduction

Developing environmentally friendly and renewable energy sources is essential due to the environmental and energy security issues caused by traditional combustion of fossil fuel-based feedstocks. Therefore, as a clean and sustainable energy carrier, hydrogen has attracted great attention in recent years [1,2]. In this regard, water electrolysis utilizing renewable energy sources to produce hydrogen is considered one of the most promising technologies [3,4]. The performance of the PEM water electrolyzer relies mainly on the properties of the membrane electrode assembly (MEA) [5], which transfers not only the protons from anode to cathode but also the reactants and products on both sides. The properties of the MEA could be affected by many parameters such as the operating temperature, pressure or current density, etc., which have been widely investigated in literatures [6–8]. Another important factor worthy of great attention
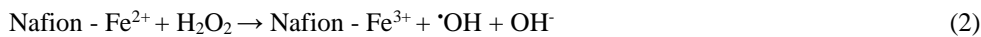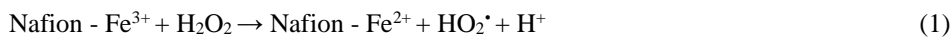
is the metal ions that can be found in the circulating water, which could severely degrade the MEA performance during the operation of a PEM water electrolyzer [9,10].

Investigations of metal ions contamination have been extensively carried out in the sister technology of PEM fuel cells. Studies show that trace amount of cations in an operating PEM fuel cell can cause significant cell performance degradation and even sudden cell failure. Li et al. [11] investigated the performance degradation of a PEM fuel cell with metal ions contamination and found that 5 ppm Fe^{3+} ions could lead to a sudden cell death and cause severe membrane damage due to the radicals produced by the catalyzed Fenton reaction. Furthermore, they also found that the Al^{3+} ions introduced into PEM fuel cell could change the reaction kinetics and mechanisms of oxygen reduction. Pozio et al. [12] studied the Nafion membrane degradation in a single cell test which utilize stainless steel316 as end plates and found that the iron ions originated from the end plates can lead to polymer degradation by catalyzing the modified Fenton reaction as follows:

$$Nafion - Fe^{3+} + H_2O_2 \rightarrow Nafion - Fe^{2+} + HO_2^\bullet + H^+ \tag{1}$$

$$Nafion - Fe^{2+} + H_2O_2 \rightarrow Nafion - Fe^{3+} + {}^\bullet OH + OH^- \tag{2}$$

$$H_2O_2 + {}^\bullet OH \rightarrow H_2O + HO_2^\bullet \tag{3}$$

The influence of Ca^{2+} contamination on fuel cell performance was investigated by Charles et al. [13], both experimentally and numerically, and results showed that the Ca^{2+} ions could accumulate on the cathode and hinder the proton transportation from anode to cathode, which then results in cathode catalyst layer thinning due to carbon corrosion. Some other studies also mentioned that Cu^{2+} ions could cause severe MEA degradation by catalyzing the Fenton reaction [14,15]. Other cations such as Mg^{2+}, Na^+, etc., have also been shown to severely affect the reaction kinetics, ion transport properties of the membrane and the thermodynamics of PEM fuel cells [16–19].

Since the state-of-the-art membrane materials used in PEM water electrolyzer are the same as those used in PEM fuel cells, the effect of the impurities on the durability and stability of membrane electrode assembly in water electrolysis are expected to be similar. However, since the operating conditions and some of the materials surrounding the membrane in PEM WE are different compared to PEM fuel cells, a dedicated investigation of the effect of impurities is necessary. Zhang et al. [20,21] studied the contamination effects of Na^+ on PEM WE and found that Na^+ could poison the electrodes severely [20,21]. Wang et al. [22] investigated the effect of iron contamination on water electrolyzer and showed that Fe^{3+} impurity could severely degrade a PEM WE cell. In our previous study, where the effect of Fe^{3+} ions contamination on a PEM water electrolyzer were tested between 1 ppm and 10 ppm, it was found that even 1 ppm Fe^{3+} contamination

can cause severe performance degradation and the degrading effects exacerbated with increasing concentration of contaminant [23,24]. In another experimental work combined with modeling [25], it was reported that iron ions can catalyze the Fenton reaction, which plays an important role in PEM water electrolyzer degradation. The authors proposed that other metallic impurities like Cu^{2+} ions in the system could also catalyze the Fenton reaction.

In this study, the contamination effect of Fe^{3+}, Cu^{2+} and Al^{3+} ions on a PEM WE unit cell were investigated. These cations were chosen as they can be present in the electrolyzer system from stack component materials and corrosion of pipes in the system [22,26,27].The concentration of the contamination ions was set to 5 ppm, and their sulphate solution were introduced into deionized water and fed to the PEM water electrolysis cell. A test without cations contamination was also carried out as a reference test. The cell performance under different impurity contaminations are studied and the corresponding possible degradation mechanisms are analyzed.

2. Experimental

2.1 Membrane electrode assembly

The cell is a sandwich structure consisting of MEA, flow fields, power connection boards and end plates on both sides, fixed with nuts and screws, as shown in Fig. 1. The membrane electrode assemblies (MEAs) and the test set-up used in the experiment are the same as the ones used in our previous studies [23,24].The MEAs consist of 0.3 mg cm^{-2} of IrO_2 that serves as the anode catalyst, Nafion®117 as the proton exchange membrane, 0.5 mg cm^{-2} of Pt/C as the cathode catalyst and a carbon cloth (Sigracet 35 DC) as the cathode side porous transport layer. The anode transport layer is a 350 µm thick Ti felt which has a porosity of 81% and the fiber diameter is 20 µm. The active area of the MEAs is 2.89 cm^2 (1.7 cm ×1.7 cm).
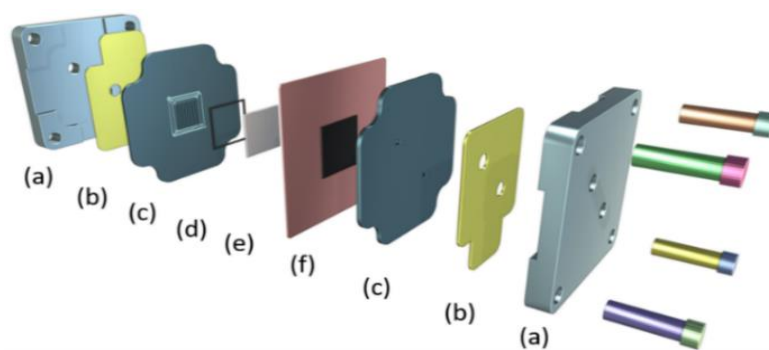

Fig. 1. Cell assembly (a) end plates, (b) power connection boards, (c) flow fields, (d)gasket, (e) Ti felt, (f) MEA.

The compression pressure was kept at 2.61 MPa by controlling the spring length on the screws. The feed solution was circulated between the anode side and the water tank, which was heated by a heater to keep a constant temperature of the cell. The flow rate of the feed solution was 270 mL min^{-1}.

2.2 Test procedures

A Gamry Reference 3000 potentiostat/galvanostat with a booster was used both as a power supply and for the electrochemical measurements. The detailed test procedure is shown in Table 1. As can be seen, prior to each test, the cell was run with DI water at a constant temperature of 60 °C and current density of 1 A cm^{-2} for 72 h to allow it to break-in. After the break-in procedure, the cell kept running at the same

DI water test	Cations contamination test (Fe^{3+}, Cu^{2+}, Al^{3+})
Step 1: Break-in for 72 h	**Step 1:** Break-in for 72 h
Step 2: DI water operation for 24 h	**Step 2:** DI water operation for 24 h
Step 3: Baseline polarization and EIS measurement	**Step 3:** Baseline polarization and EIS measurement
Step 4: DI water operation of 144 h with polarization and EIS measurement at different test points	**Step 4:** Cations were introduced into the feed solution
	Step 5: Contamination operation of 264 h with polarization and EIS measurement at different test points

Table 1 Operation modes.

operating conditions for a reference DI water test for 144 h. For contamination test, 5 ppm contamination solutions were prepared in advance by introducing the sulfate solution of target particles (Fe$_2$(SO$_4$)$_3$, CuSO$_4$, Al$_2$(SO$_4$)$_3$) into DI water. In this case, the break-in procedure was followed by a 24 h operation with DI water and then the DI water tank (bottle) was replaced by the tank filled with the corresponding contaminant solution. The cell was run at 60 °C and 1 A cm^{-2} during the whole contamination test period. To better investigate the degradation effects of the impurities on cell performance, the contamination tests were done for 264 h.

2.3 Characterization techniques

Polarization curves and electrochemical impedance spectroscopy (EIS) measurements were carried out every 24 h after break-in procedure during each test according to the test procedures described above. The voltage was varied from 1 V to 2.5 V for the polarization tests. The sweeping frequency of the galvanostatic EIS measurements was from 100 kHz to 0.01 Hz with 10 measurements points recorded per decade. The microstructural changes in the cross-section of the MEAs and impurities distribution on the MEAs were examined by Scanning Electron Microscopy (SEM) and Energy Dispersive X-ray Spectroscopy (EDX) measurements.

In order to depict the EIS results more intuitively, an equivalent circuit (EC) model shown in Fig. 2 was employed to simulate the EIS data. In Fig. 2, R_Ω represents the total ohmic resistance of the single cell and R_{HF} represents the high frequency resistance, which is dominated by the electrochemical reaction processes on both sides, especially the anode side because of the fast kinetics on cathode side [28]. R_{LF} represents the low frequency resistance, which is dominated by mass transfer activities [29]. Taking into account surface roughness and the non-uniformly distributed double layer capacitance of electrolyzer and to reduce the deviation between data and model fits, two constant phase elements (CPE_1, CPE_2), in parallel with R_{HF} and R_{LF}, respectively, were employed to represent the double layer capacitances [30,31]. The impedance of a CPE is defined as:

$$Z_{CPE}(\omega) = Q^{-1}(j\omega)^{-\alpha} \tag{4}$$

where ω is the frequency (rad s^{-1}), Q is the pseudo-capacitance, α is the power coefficient of CPE, which varies from 0 to 1 and determines the CPE nature [32]. α is normally kept constant for all fits, except in some cases when the current varies [33]. In this work since the current is constant, the α values were fixed at 0.5 for CPE_1 (high frequency semicircular arc) and 0.7 for CPE_2 (low frequency semicircular arc). The "goodness of fit", χ^2, for all the fits in this work was in the order of 10^{-6}, which is well below the 10^{-4} criterion for a good fit indicated by Gamry for their fitting algorithm [34], where the smaller the value the better the fit.
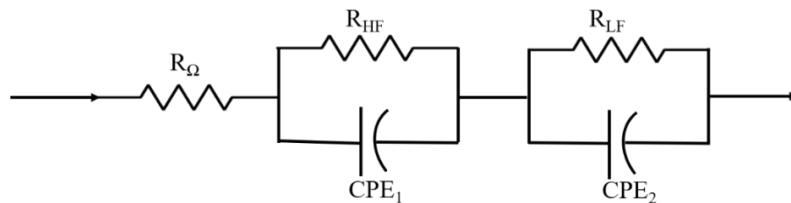

Fig. 2. (a) Equivalent circuit model, (b) Fit between the EIS and equivalent circuit.

3. Results and discussion

3.1 Effects of 5 ppm Fe^{3+}, Cu^{2+} and Al^{3+} contamination on cell performance

After 3 days of break-in procedure, the cell operated for 24 h with DI water and then EIS and polarization measurements were carried out before the contamination tests were started. The results were recorded as reference for each cell for comparison with the contamination tests. The cell performance changes with different contaminants are shown in Fig. 3 (a). Even though the MEAs used in this study have the same composition of materials for different components, it can be seen that there are differences among the initial performance of the cells before the impurities were introduced. These differences could be both due to small non-uniformities from the MEA manufacturing processes and minor differences in the manual assembly process. Nonetheless, the effects of the contamination tests can be clearly seen by observing the voltage profile and polarization curves of each test.
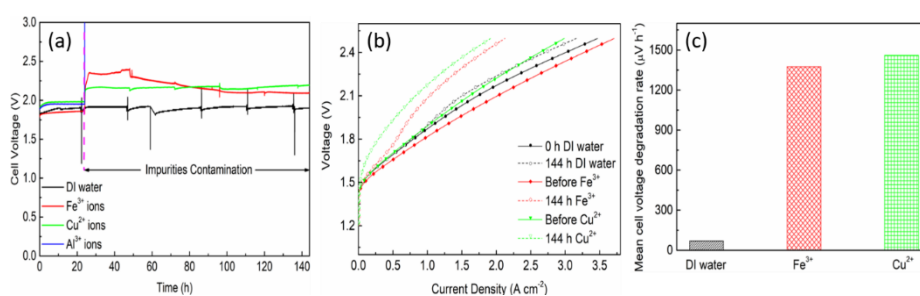

Fig. 3. Performance and degradation, (a) Cell voltage profile for the different tests, (b) Polarization curves after break-in and at the end of test for all tests and (c) Mean cell voltage degradation rates at 1 A cm^{-2}.

As shown in Fig. 3 (a), the cell performance changes only slightly for the DI water operating, increasing from 1.88 V at the beginning of test to 1.9 V at the end. However, the performance decreased dramatically when both Fe^{3+} and Cu^{2+} ions were introduced into the anode feed. After the initial decrease, the performance recovered continuously throughout the test period in the case of Fe^{3+} and decreased slightly for Cu^{2+}. The cell voltage increased sharply from 1.85 V to 2.356 V when Fe^{3+} ions were introduced into the DI water as feed solution but then first experienced a slight increase up to 2.4 V followed by a gradual decrease to 2.07 V at the end of the test. For Cu^{2+}, the cell voltage increased from 1.9 V to 2.17 V immediately after Cu^{2+} ions were introduced. Unlike in the case of Fe^{3+} contamination, the cell voltage then increased slightly and reached 2.218 V at the end of the contamination test, representing a continuous but modest decrease in cell performance after the rapid initial performance loss. It can be seen that both Fe^{3+} and Cu^{2+} induce similarly significant performance degradations during the duration of the tests.

The mean voltage degradation rate of each cell during the test duration (144 h for comparison) was calculated in order to compare the changes in cell performance due to different contamination conditions, which was shown in a bar graph of Fig. 3 (c). All three operation modes show positive mean cell degradation rate, which means performance

degradation took place after each of the tests. The mean cell voltage degradation rate for DI water is 0.135 mV h $^{-1}$ and the mean cell voltage degradation rates for Fe^{3+} and Cu^{2+} are 1.375 mV h $^{-1}$ and 1.460 mV h $^{-1}$, around 10 and 11 times higher than DI water, respectively.

A much more severe cell performance decay was observed when Al^{3+} ions were introduced. The cell voltage increased drastically from 1.91 V to 5.32 V in less than 1 min, and the cell failed immediately. The 5 ppm Al^{3+} contamination test was repeated twice and a lower concentration of 3 ppm contamination test was also carried out, but similar results of sudden cell failure took place. Therefore, further analysis of Al^{3+} contamination on cell performance was not possible, but SEM and EDX measurements were done on the MEA for post-mortem analysis.

3.2 Reference DI water test

As a baseline reference for the contamination tests, the single cell was first operated with DI water as the feed solution at the temperature of 60 °C and current density of 1 A cm $^{-2}$ for 144 h. The obtained results are shown in Fig. 4. Even though the performance remains unchanged throughout the test period below 1 A cm $^{-2}$, a small performance decay is seen after this point. This implies that even under DI water operation the performance decay with time is enhanced at higher current densities. However, this decrease in performance seems to stabilize with time and the degradation rate becomes comparatively less pronounced in the later stages of the test period.
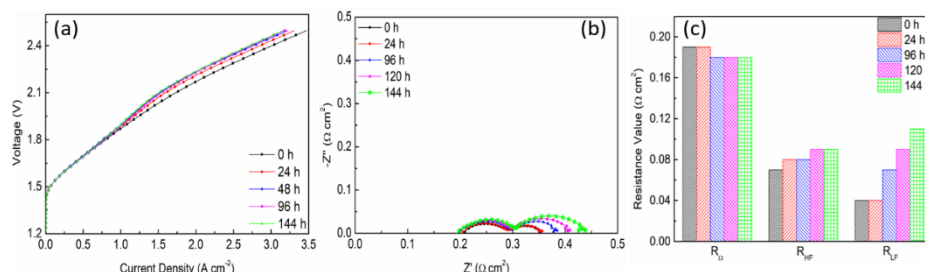
Fig. 4. Reference DI water tests, (a) Polarization curves, (b) Electrochemical impedance spectra and (c) Fitted resistances.

The Nyquist plots of the DI water test are shown in Fig. 4 (b), where two distinct semicircular arcs are visible. It can be seen that the second arc enlarges increasingly, while the first arc and the high frequency intercept remain almost unaltered for the test period.

The resistance values obtained after fitting the EIS data to the EC model for DI water are shown in Fig. 4 (c). It can be seen that the ohmic resistance remained almost unaltered during the whole test. The high frequency resistance and low frequency increased slightly during the test duration. These resistance values are employed as reference for the changes observed during the cationic contamination tests.

3.3 Fe^{3+} contamination analysis

The performance trends observed from the voltage profiles in Fig. 3 (a) were further studied by analyzing the polarization curves obtained at different test points during contamination tests. As shown in Fig. 5 (a), the cell performance decreased dramatically after the first 24 h of Fe^{3+} ions contamination test, but then progressively recovered until the end of test. It can also be noticed that the performance recovery was more pronounced in the intermediate stages of the tests than in the end, which leads to believe that full performance recovery may not be possible as the overall cell performance at the end of the test seems to stabilize at higher voltages than in the beginning of test. The performance decay may be attributable to the higher affinity of Fe^{3+} than H^+ for SO_3- group in the Nafion membrane, which decreases the effective triple-phase boundaries and the proton conductivity [22,35]. Moreover, Wang et al. [22] showed that Fe^{3+} ions migrate from the anode to the cathode and therefore, the decrease in triple-phase boundaries may occur on both sides. However, they also showed that Fe^{3+} flowed out of the electrolyzer and some of it was reduced to Fe^{2+}, which may explain the partial performance recovery during the Fe^{3+} tests. Fe^{3+} ions on Nafion membrane may also catalyze the Fenton reaction, which could generate hydroxyl radicals that may attack the membrane [11].
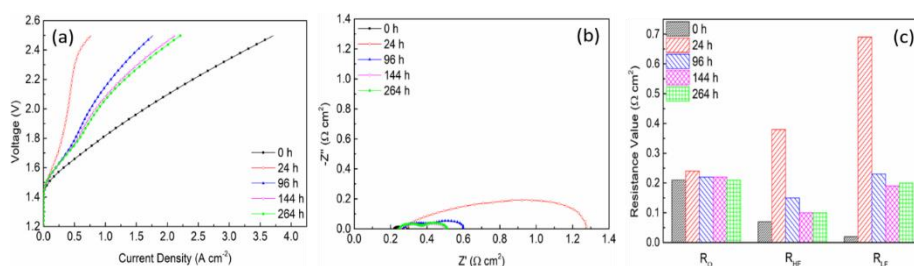

Fig. 5. Fe^{3+} contamination tests (a) Polarization curves, (b) Electrochemical Impedance Spectra and (c) Fitted resistances.

To further elucidate the performance change of the single cell, EIS measurements were also carried out at different test points. The obtained Nyquist plots are shown in Fig. 5 (b), where two semicircular arcs can be seen. The high frequency intercept on the real axis first increased slightly after the Fe^{3+} ions were introduced into the cell and then after a small decrease it remained almost unaltered for most of the duration of the tests. The size and diameter of the semicircular arcs on the other hand increased dramatically in the beginning and gradually recovered during the remainder of the test. This reflects that most of the performance changes previously described from the voltage profile in Fig. 3 (a) and polarization curves in Fig. 5 (a) for Fe^{3+} contamination tests are attributable to the processes associated with the semicircular arcs, i.e., reaction kinetics and concentration losses, and not the high frequency intercept on the real axis, mainly dominated by the proton conductivity.

The resistance values obtained by fitting the EIS data to the EC model are provided in Fig. 5 (c). It can be seen that the value of R_Ω slightly increased from 0.21 Ω cm^2 to 0.24 Ω cm^2 after 24 hours of Fe^{3+} ions contamination test, then decreased with time and stabilized at 0.20 Ω cm^2 at the end of the test, which is close to the initial value. The increase in ohmic resistance after introducing the Fe^{3+} ions into the cell could be mainly due to the high affinity of Fe^{3+} ions for the sulfonic acid groups than protons, whereby the Fe^{3+} ions can substitute H^+ occupying the ion exchange sites of the membrane and thus hinder the transportation of the protons, leading to increased R_Ω value [5,22,36]. Michael et al. [35] reported that Fe^{3+} ions decrease ionic conductivity of the membrane. Moreover, the Fe^{3+} ions could migrate from anode to cathode due to concentration and potential differences [22]. This could catalyze the Fenton reaction, thereby promoting the production of radicals such as OH$^•$, H$^•$ on both electrodes[11,25] that may attack the membrane, resulting in the membrane thinning phenomenon [37,38]. The fact that the ohmic resistance at the beginning and end of the test are almost identical seems to indicate that the expected thinning due to radicals formation is not significant. However, other factors, such as the Fe^{3+} ion replacement of the protons, occupying ion exchange cites of the membrane, could be counteracting the effects of membrane thinning on the ohmic resistance. If this is the case, the performance recovery seen across all the resistances may be only temporary as the membrane degradation will inevitably impact the cell's lifetime negatively.

In Fig. 5 (c), it can be seen that the high frequency resistance of the single cell increased dramatically from 0.07 Ω cm^2 to 0.38 Ω cm^2 after 24 hours of Fe^{3+} ions contamination test and then decreased gradually to 0.12 Ω cm^2 at the end of test. This is in line with the notion that foreign metallic ions have better affinity with the sulfonic acid groups in Nafion than H^+, which reduces the effective triple-phase boundaries, thereby increasing the activation overpotential [19,39,40]. Furthermore, due to the Fe^{3+} migration from the anode to the cathode, this phenomenon is expected to slow the reaction kinetics on both electrodes, which may explain the dramatic initial increase in the associated R_{HF}. However, Fe^{3+} ions are also reported to continuously exit the electrolyzer rather than accumulate in the catalyst layer [22]. This may have led to the subsequent decrease in R_{HF}.

Likewise, the low frequency resistance also shows dramatic initial increase followed by significant recovery. This too, could be the result of reduced effective triple-phase boundaries, which could lead to higher concentration overpotential [9,22]. Fe^{3+} ions introduced into the cell can accumulate on the anode catalyst layer, thereby occupying effective catalyst sites and poisoning the electrocatalysts [20]. The loss of active area and adsorption on the anode catalyst surface could then decrease the reaction kinetics of oxygen evolution and hinder the release of the product, thereby leading to increase in charge and mass transfer resistance. However, the Fe^{3+} ions could also transfer from anode to cathode under the voltage difference and concentration gradient, and even exit the electrolyzer as mentioned above, which could alleviate

the activation and concentration overpotential on the anode, contributing to the charge and mass transport recovery. The recovery becomes less pronounced at the later stages of the test both for R_{HF} and R_{LF}, which could be due to the fact that the distribution of Fe^{3+} ions between the MEA and feed solution reaches equilibrium with time.

3.4 Cu^{2+} contamination analysis

The effect of 5 ppm Cu^{2+} contamination on the single cell performance are shown in Fig. 6 (a). Similarly to Fe^{3+} ions, the presence of Cu^{2+} causes significant performance decay in the first 24 h. However, unlike with Fe^{3+}, where the initial decay was followed by performance recovery, the performance decay continued slowly throughout the remainder of the tests in the case of Cu^{2+}. It can also be noticed that the initial dramatic performance decay is more pronounced for Fe^{3+} than for Cu^{2+}. Okada et al. [19] reported that though impurity cations have a high preference over H^+ in Nafion membranes, the order of preference is $Fe^{3+} > Ni^{2+} > Cu^{2+}$, which may explain why the initial performance decay is lower for Cu^{2+} than Fe^{3+}. However, it is also reported that Cu^{2+} adsorbs into the membrane more readily than Fe^{3+} [35], and tends to stay in the membrane unlike Fe^{3+}, which is reported to exit the electrolyzer continuously [22]. This implies that though the initial degrading effects are less compared to Fe^{3+} due to the lower affinity of Cu^{2+} to Nafion than Fe^{3+}, the performance decay in the presence of Cu^{2+} continues throughout the tests due to its higher adsorption properties, and therefore, no performance recovery is seen.
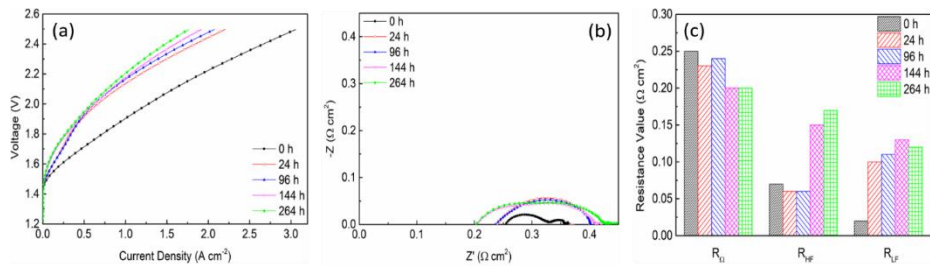

Fig. 6. Cu^{2+} contamination tests (a) Polarization curves, (b) Electrochemical Impedance Spectra and (c)fitted resistances.

As can be seen in Fig. 6 (b), unlike for Fe^{3+} contamination, the high frequency intercept on the real axis decreased with time significantly, implying decreased ohmic resistance, while the diameter of the first semicircular arc enlarged. From the fitted resistance values given in Fig. 6 (c) it can be seen that in the presence of Cu^{2+} the overall ohmic resistance decreases with time. This may be attributed to the increased mobility of protons in the presence of Cu^{2+} ions [19]. According to Okada et al. [19] in the presence of Fe^{3+}, the mobility of H^+ decreases sharply (retardation mode), but in the presence of Cu^{2+}, the mobility of H^+ increases almost linearly with the amount of Cu^{2+} (acceleration mode). Even though the observed decrease in ohmic resistance due to Fe^{3+} not as sharp, the opposite effects of Fe^{3+} and Cu^{2+} on the mobility of H^+ are confirmed by the trends of R_Ω in the current work. Moreover, it has been reported that Cu^{2+} ions are also Fenton

active ions and can catalyze the Fenton reaction [15,41], which can cause membrane thinning due to radical attack that can in turn contribute to the decrease in ohmic resistance.

On the other hand, both R_{HF} and R_{LF} increased significantly in the presence of Cu^{2+}. As previously mentioned, impurity cations have higher affinity to Nafion than H^+, though more so for Fe^{3+} than Cu^{2+}, similar effects of reduced effective triple-phase boundaries may be expected. This in turn could lead to similar increase in activation and concentration overpotentials. However, since Cu^{2+} has higher adsorption rate on the membrane than Fe^{3+}, the degrading effects continue in time in the presence of Cu^{2+}. Moreover, Cu^{2+} ions like Fe^{3+} ions could also migrate from the anode to the cathode under the concentration gradient and voltage differences, where they could be reduced to Cu as Cu^{2+} ions have positive Nernst potential [9]. The produced Cu could then accumulate on the catalyst layers, covering the active catalyst sites, leading to the increase in charge transfer resistance and mass transfer resistance[22,42].

3.5 Post-mortem analysis

SEM measurements were carried out on the cross-section of the MEAs after all the electrochemical tests to investigate the degradation mechanisms on the membranes and catalyst layers. Figure 7 shows the SEM images of all the MEAs after the tests. It can be seen that the membrane thicknesses for the different tests are different at 151.8 µm, 175.7 µm and 202.6 µm for DI water test, Fe^{3+} and Cu^{2+}, respectively. It is worth noting that the initial ohmic resistances of the MEAs used for the different tests were also different among each other, corresponding to 0.19 Ω cm^2 for DI water, 0.21 Ω cm^2 for Fe^{3+} and 0.25 Ω cm^2 for Cu^{2+}. A correspondence can be noticed between the initial resistances and final thicknesses of the different MEAs, with resistance and thickness order of DI water $<$ Fe^{3+} $<$ Cu^{2+}. However, in the absence of initial membrane thicknesses it is not possible to conclude on the effect of the contaminants on the membrane thickness. Since the MEAs are commercial, it was not possible to know a priori the thicknesses of the fresh membranes, which makes the post-mortem analysis difficult if there is not guarantee of reproducibility of the manufacturing processes. It was assumed in the beginning of test that they would have comparable thicknesses, but this does not seem to be the case as manifested by the different initial performances of the cells and the different initial ohmic resistances.

When looking into the catalyst layer, the recorded anode catalyst layer thicknesses are 5.806 µm, 9.602 µm, 10.33 µm for DI water, Fe^{3+} and Cu^{2+}, respectively. The cathode catalyst layer thicknesses are 18.76 µm of DI water test, 7.146 µm and 6.978 µm for Fe^{3+} and Cu^{2+}. Although it is difficult to compare the catalyst layer thickness due to the lack of the initial values, it is believed that catalyst dissolution may occur on both sides in the presence of Fe^{3+} and Cu^{2+} ions. It is reported that the anode catalyst IrO_2 starts to become soluble when the potential is at approximately 1.8 V and the Pt/C

degrades even at a cathode potential less than 0 V [26]. The migrated Fe^{3+} and Cu^{2+} ions in the catalyst layers can occupy the ionomer and block the active surface sites of the catalyst layers, leading to the cell overpotential increase on both sides. Although the IrO_2 is a relatively stable anode catalyst, the oxidation environment and high overpotential caused by cations contamination at the anode could lead to the dissolution of IrO_2 [26,43]. In addition, Pt has high sensitivity to metallic impurities, where underpotential deposition (UPD) at the catalyst surface may lead to high cathode overpotential (> 0 V) [42,44], which could in turn result in cathode catalyst dissolution.
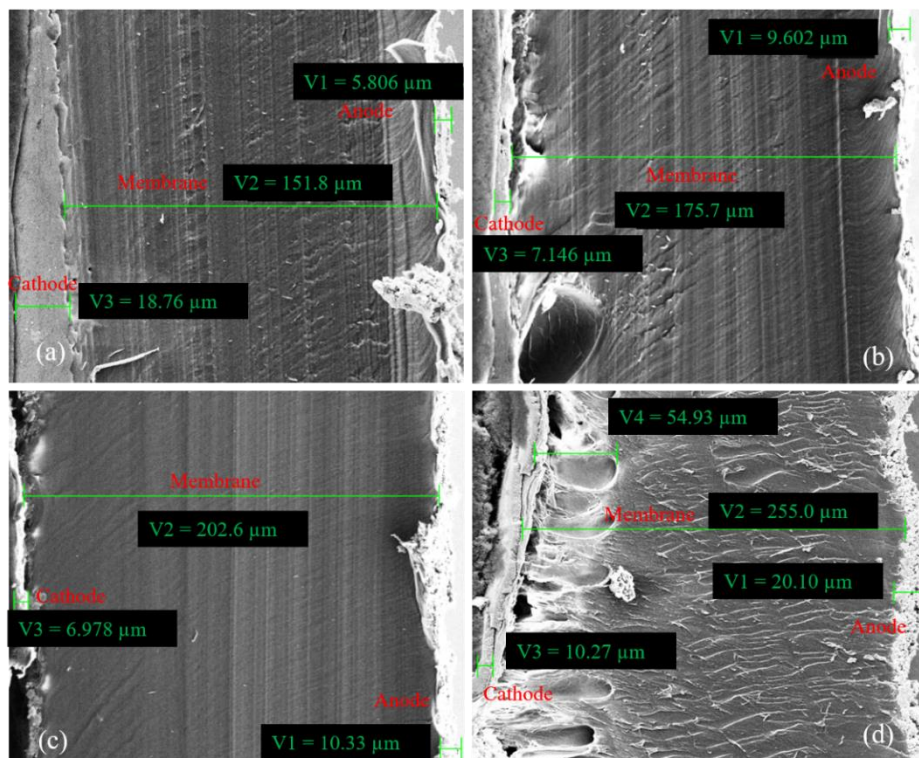

Fig. 7. SEM images of MEAs under the operating condition of (a) DI water, (b) Fe^{3+} contamination, (c) Cu^{2+} contamination and (d) Al^{3+} contamination.

Although the electrochemical test of Al^{3+} contamination could not be done due to the sudden cell failure, the post-mortem analysis of the MEA were carried out through SEM measurement as shown in Fig. 7 (d). It can be seen that a series of small cavities with diameters of about 54.93 µm appeared on the membrane close to the cathode side. These cavities may be formed by cathode catalyst layer dissolution which is followed by transport into the membrane [10], and may gradually became pinholes during the Al^{3+} contamination [9],[27]. Even though no pinholes can be seen in the examined section of the MEA it cannot be ruled out that these perforations develop into pinholes. Therefore, these cavities may be the main reason that lead to the sudden cell failure.
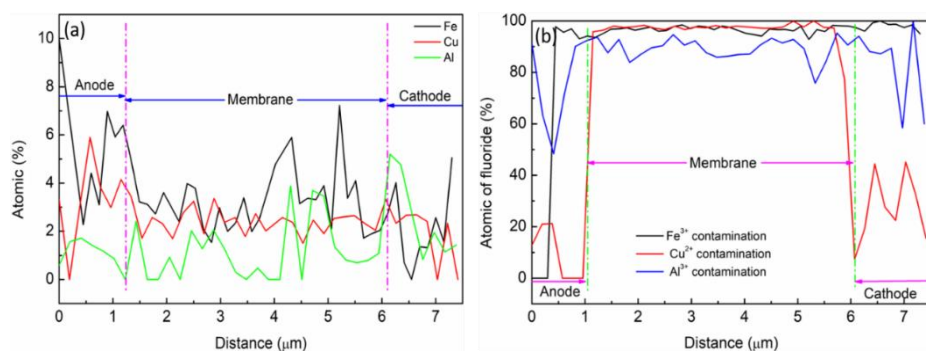
Fig. 8. EDX of the distribution of impurity ions and fluoride at the cross-section of the contaminated MEAs.

Finally, EDX measurements of impurities and fluoride distribution were also carried out. As shown in Fig. 8 (a), all the impurity ions are distributed not only on the membrane but also on both of the catalyst layers. This confirms that the impurity ions migrate from the anode side through membrane to the cathode side and deposit on the electrocatalysts [9,22]. The atomic percentage of Fe^{3+} ions and Cu^{2+} ions on the anode side is larger than that at the membrane and cathode side, representing more agglomeration of Fe^{3+} ions and Cu^{2+} ions on the anode side. This could be the reason for the thicker anode catalyst layers for the impurity tests compared to the DI water test. However, the atomic percentage of Al^{3+} ions on the cathode side and membrane close to the cathode side is larger than that on the anode and the membrane close to the anode side. This implies that more Al^{3+} ions migrated to the cathode side leading to more severe cathode side degradation, which is also seen by the presence of crater like formations on the membrane close to the cathode catalyst layer in the SEM image in Fig. 7 (d).

Fig. 8 (b) shows the fluoride distribution on the cross-section of the MEAs. As part of the Nafion membrane, fluoride should be present all through the membrane but should not be present on the catalyst layers. Therefore, fluoride detected on the catalyst layers could be an indication that fluoride must be released from the membrane. Fluoride release as a signal of membrane attacked caused by Fenton reaction, which contributes to membrane thinning, has been widely studied in the literature [23,33]. As can be seen in Fig. 8 (b), the fluoride is present not only on the membrane but also the on the anode and the cathode side of the MEAs after the contamination tests, implying membrane degradation due to the impurity ions. The atomic fluoride release percentage on the anode and cathode side for Cu^{2+} ions is lower than that of Fe^{3+} and Al^{3+} ions, illustrating that the degradation effect of Fe^{3+} and Al^{3+} ions were more severe than the effects of Cu^{2+} ions.

4. Conclusion

The effects of 5 ppm of Fe^{3+}, Cu^{2+} and Al^{3+} ions on the performance of a PEM water electrolysis single cell were investigated by introducing the corresponding sulfate solution of the three cations into the feed water. Results of the

polarization curves and EIS measurements showed that all the impurity ions degraded the cell performance severely. It was found that though the initial degrading effects of Fe^{3+} are higher than those of Cu^{2+}, a significant performance recovery is seen during the Fe^{3+} tests while the performance decay continued without recovery in the case of Cu^{2+}. This is attributed to the fact that Cu^{2+} adsorbs into the membrane more readily than Fe^{3+} and tends to stay in the membrane unlike Fe^{3+}, which is reported to exit the electrolyzer continuously.

The fitted resistance values show that mainly the charge and mass transfer resistance increased significantly both for Fe^{3+} and Cu^{2+} due to the higher preference of impurity cations over H^+ in Nafion membranes that can reduce the triple-phase boundaries, thereby increasing the activation and concentration overpotentials. Similarly to the performance trends, the charge and mass transfer resistances continuously recovered after an initial dramatic increase in the case of Fe^{3+}, but continuously increased for Cu^{2+}.

The EDX results showed that Fe^{3+}, Cu^{2+} and Al^{3+} ions could transfer from anode to cathode and deposit on the membrane and catalyst layers, which may cover the active catalyst sites, poison the electrodes and degrade the catalyst ionomer layers.

Another important finding of this work is that the existence of Al^{3+} ions in the circulating water could lead to severe cathode side catalyst layer degradation and sudden cell failure even at low concentration of 3 ppm. Therefore, aluminum materials should be avoided in a PEM water electrolysis system.

Acknowledgments

Reference

[1]   C. Acar, I. Dincer, Review and evaluation of hydrogen production options for better environment, Journal of Cleaner Production. 218 (2019) 835–849. https://doi.org/10.1016/j.jclepro.2019.02.046.

[2]   S.M.M. Ehteshami, S.H. Chan, The role of hydrogen and fuel cells to store renewable energy in the future energy network – potentials and challenges, Energy Policy. 73 (2014) 103–109. https://doi.org/10.1016/j.enpol.2014.04.046.

[3]   F. Barbir, PEM electrolysis for production of hydrogen from renewable energy sources, Solar Energy. 78 (2005) 661–669. https://doi.org/10.1016/j.solener.2004.09.003.

[4]   S. Shiva Kumar, V. Himabindu, Hydrogen production by PEM water electrolysis – A review, Materials Science for Energy Technologies. 2 (2019) 442–454. https://doi.org/10.1016/J.MSET.2019.03.002.

[5]   J. Mo, S. Steen, Z. Kang, G. Yang, D.A. Taylor, Y. Li, T.J. Toops, M.P. Brady, S.T. Retterer, D.A. Cullen, J.B. Green, F.Y. Zhang, Study on corrosion migrations within catalyst-coated membranes of proton exchange membrane electrolyzer cells, International Journal of Hydrogen Energy. 42 (2017) 27343–27349. https://doi.org/10.1016/j.ijhydene.2017.09.020.

[6]   M. Chandesris, R. Vincent, L. Guetaz, J.S. Roch, D. Thoby, M. Quinaud, Membrane degradation in PEM fuel cells: From experimental results to semi-empirical degradation laws, International Journal of Hydrogen Energy. 42 (2017) 8139–8149. https://doi.org/10.1016/j.ijhydene.2017.02.116.

[7]   C. Immerz, M. Schweins, P. Trinke, B. Bensmann, M. Paidar, T. Bystroň, K. Bouzek, R. Hanke-Rauschenbach, Experimental characterization of inhomogeneity in current density and temperature distribution along a single-channel PEM water electrolysis cell, Electrochimica Acta. 260 (2018) 582–588. https://doi.org/10.1016/j.electacta.2017.12.087.

[8]   S. al Shakhshir, X. Cui, S. Frensch, S.K. Kær, In-situ experimental characterization of the clamping pressure effects on low temperature polymer electrolyte membrane electrolysis, International Journal of Hydrogen Energy. 42 (2017) 21597–21606. https://doi.org/10.1016/j.ijhydene.2017.07.059.

[9]   S. Sun, Z. Shao, H. Yu, G. Li, B. Yi, Investigations on degradation of the long-term proton exchange membrane water electrolysis stack, Journal of Power Sources. 267 (2014) 515–520. https://doi.org/10.1016/j.jpowsour.2014.05.117.

[10]   S.A. Grigoriev, K.A. Dzhus, D.G. Bessarabov, P. Millet, Failure of PEM water electrolysis cells: Case study involving anode dissolution and membrane thinning, International Journal of Hydrogen Energy. 39 (2014) 20440–20446. https://doi.org/10.1016/j.ijhydene.2014.05.043.

[11]   H. Li, K. Tsay, H. Wang, J. Shen, S. Wu, J. Zhang, N. Jia, S. Wessel, R. Abouatallah, N. Joos, J. Schrooten, Durability of PEM fuel cell cathode in the presence of Fe^{3+} and Al^{3+}, Journal of Power Sources. 195 (2010) 8089–8093. https://doi.org/10.1016/j.jpowsour.2010.07.003.

[12]   A. Pozio, R.F. Silva, M. de Francesco, L. Giorgi, Nafion degradation in PEFCs from end plate iron contamination, Electrochimica Acta. 48 (2003) 1543–1549. https://doi.org/10.1016/S0013-4686(03)00026-4.

[13]   C.J. Banas, Md.A. Uddin, J. Park, L.J. Bonville, U. Pasaogullari, Thinning of Cathode Catalyst Layer in Polymer Electrolyte Fuel Cells Due to Foreign Cation Contamination, Journal of The Electrochemical Society. 165 (2018) F3015–F3023. https://doi.org/10.1149/2.0021806jes.

[14]   X. Cheng, Z. Shi, N. Glass, L. Zhang, J. Zhang, D. Song, Z.S. Liu, H. Wang, J. Shen, A review of PEM hydrogen fuel cell contamination: Impacts, mechanisms, and mitigation, Journal of Power Sources. 165 (2007) 739–756. https://doi.org/10.1016/j.jpowsour.2006.12.012.

[15]   M. Inaba, Degradation Mechanism of Polymer Electrolyte Fuel Cells, 14th International Conference on the Properties of Water and Steam in Kyoto. (2004) 395–402.

[16]   J. Zhu, J. Tan, Q. Pan, Z. Liu, Q. Hou, Effects of Mg^{2+} contamination on the performance of proton exchange membrane fuel cell, Energy. 189 (2019) 116135. https://doi.org/10.1016/J.ENERGY.2019.116135.

[17]   M.A. Uddin, J. Qi, X. Wang, U. Pasaogullari, L. Bonville, Distributed cation contamination from cathode to anode direction in polymer electrolyte fuel cells, International Journal of Hydrogen Energy. 40 (2015) 13099–13105. https://doi.org/10.1016/j.ijhydene.2015.07.134.

[18]   X. Wang, J. Qi, O. Ozdemir, A. Uddin, U. Pasaogullari, L.J. Bonville, T. Molter, Ca^{2+} as an Air Impurity in Polymer Electrolyte Membrane Fuel Cells, Journal of The Electrochemical Society. 161 (2014) F1006–F1014. https://doi.org/10.1149/2.0561410jes.

[19]   T. Okada, Y. Ayato, M. Yuasa, I. Sekine, The effect of impurity cations on the transport characteristics of perfluorosulfonated ionomer membranes, Journal of Physical Chemistry B. 103 (1999) 3315–3322. https://doi.org/10.1021/jp983762d.

[20]   L. Zhang, X. Jie, Z.G. Shao, Z.M. Zhou, G. Xiao, B. Yi, The influence of sodium ion on the solid polymer electrolyte water electrolysis, International Journal of Hydrogen Energy. 37 (2012) 1321–1325. https://doi.org/10.1016/j.ijhydene.2011.10.023.

[21]   L. Zhang, X. Jie, Z.G. Shao, X. Wang, B. Yi, The dynamic-state effects of sodium ion contamination on the solid polymer electrolyte water electrolysis, Journal of Power Sources. 241 (2013) 341–348. https://doi.org/10.1016/j.jpowsour.2013.04.049.

[22]   X. Wang, L. Zhang, G. Li, G. Zhang, Z.G. Shao, B. Yi, The influence of Ferric ion contamination on the solid polymer electrolyte water electrolysis performance, Electrochimica Acta. 158 (2015) 253–257. https://doi.org/10.1016/j.electacta.2015.01.140.

[23]   N. Li, S.S. Araya, S.K. Kær, Long-term contamination effect of iron ions on cell performance degradation of proton exchange membrane water electrolyser, Journal of Power Sources. 434 (2019) 226755. https://doi.org/10.1016/j.jpowsour.2019.226755.

[24]   N. Li, S.S. Araya, S.K. Kær, The effect of Fe^{3+} contamination in feed water on proton exchange membrane electrolyzer performance, International Journal of Hydrogen Energy. 44 (2019) 12952–12957. https://doi.org/10.1016/j.ijhydene.2019.04.015.

[25]   S.H. Frensch, G. Serre, F. Fouda-Onana, H.C. Jensen, M.L. Christensen, S.S. Araya, S.K. Kær, Impact of iron and hydrogen peroxide on membrane degradation for polymer electrolyte membrane water electrolysis: Computational and experimental investigation on fluoride emission, Journal of Power Sources. 420 (2019) 54–62. https://doi.org/10.1016/j.jpowsour.2019.02.076.

[26]   Q. Feng, X. Yuan, G. Liu, B. Wei, Z. Zhang, H. Li, H. Wang, A review of proton exchange membrane water electrolysis on degradation mechanisms and mitigation strategies, Journal of Power Sources. 366 (2017) 33–55. https://doi.org/10.1016/j.jpowsour.2017.09.006.

[27]   J. Qi, X. Wang, U. Pasaogullari, L. Bonville, T. Molter, Effect of Al^{3+} Contaminant on Polymer Electrolyte Fuel Cell Performance, Journal of The Electrochemical Society. 160 (2013) F916–F922. https://doi.org/10.1149/2.022309jes.

[28]   I. Dedigama, P. Angeli, K. Ayers, J.B. Robinson, P.R. Shearing, D. Tsaoulidis, D.J.L. Brett, In situ diagnostic techniques for characterisation of polymer electrolyte membrane water electrolysers - Flow visualisation and electrochemical impedance spectroscopy, International Journal of Hydrogen Energy. 39 (2014) 4468–4482. https://doi.org/10.1016/j.ijhydene.2014.01.026.

[29]   P. Millet, N. Mbemba, S.A. Grigoriev, V.N. Fateev, A. Aukauloo, C. Etiévant, Electrochemical performances of PEM water electrolysis cells and perspectives, International Journal of Hydrogen Energy. 36 (2011) 4134–4142. https://doi.org/10.1016/J.IJHYDENE.2010.06.105.

[30]   P. Córdoba-Torres, T.J. Mesquita, O. Devos, B. Tribollet, V. Roche, R.P. Nogueira, On the intrinsic coupling between constant-phase element parameters α and Q in electrochemical impedance spectroscopy, Electrochimica Acta. 72 (2012) 172–178. https://doi.org/10.1016/j.electacta.2012.04.020.

[31]   K. Elsøe, L. Grahl-Madsen, G.G. Scherer, J. Hjelm, M.B. Mogensen, Electrochemical Characterization of a PEMEC Using Impedance Spectroscopy, Journal of The Electrochemical Society. 164 (2017) F1419–F1426. https://doi.org/10.1149/2.0651713jes.

[32]   M.A. Blommaert, D.A. Vermaas, B. Izelaar, B. In'T Veen, W.A. Smith, Electrochemical impedance spectroscopy as a performance indicator of water dissociation in bipolar membranes, Journal of Materials Chemistry A. 7 (2019) 19060–19069. https://doi.org/10.1039/c9ta04592a.

[33]   C. Jeppesen, P. Polverino, S.J. Andreasen, S.S. Araya, S.L. Sahlin, C. Pianese, S.K. Kær, Impedance characterization of high temperature proton exchange membrane fuel cell stack under the influence of carbon monoxide and methanol vapor, International Journal of Hydrogen Energy. 42 (2017) 21901–21912. https://doi.org/https://doi.org/10.1016/j.ijhydene.2017.07.094.

[34]   Https://www.gamry.com/application-notes/EIS/equivalent-circuit-modeling-using-the-gamry-eis300-electrochemical-impedance-spectroscopy-software/.

[35]   M.J. Kelly, G. Fafilek, J.O. Besenhard, H. Kronberger, G.E. Nauer, Contaminant absorption and conductivity in polymer electrolyte membranes, Journal of Power Sources. 145 (2005) 249–252. https://doi.org/10.1016/j.jpowsour.2005.01.064.

[36]   B. Kienitz, B. Pivovar, T. Zawodzinski, F.H. Garzon, Cationic Contamination Effects on Polymer Electrolyte Membrane Fuel Cell Performance, Journal of The Electrochemical Society. 158 (2011) B1175. https://doi.org/10.1149/1.3610986.

[37]   L. Gubler, S.M. Dockheer, W.H. Koppenol, Radical (HO$^\bullet$, H$^\bullet$ and HOO$^\bullet$) Formation and Ionomer Degradation in Polymer Electrolyte Fuel Cells, Journal of The Electrochemical Society. 158 (2011) B755. https://doi.org/10.1149/1.3581040.

[38]   M. Chandesris, V. Médeau, N. Guillet, S. Chelghoum, D. Thoby, F. Fouda-Onana, Membrane degradation in PEM water electrolyzer: Numerical modeling and experimental evidence of the influence of temperature and current density, International Journal of Hydrogen Energy. 40 (2015) 1353–1366. https://doi.org/10.1016/j.ijhydene.2014.11.111.

[39]   J.G. Goodwin, K. Hongsirikarn, S. Greenway, S. Creager, Effect of cations (Na$^+$, Ca^{2+}, Fe^{3+}) on the conductivity of a Nafion membrane, Journal of Power Sources. 195 (2010) 7213–7220. https://doi.org/10.1016/j.jpowsour.2010.05.005.

[40]   T. Okada, S. Møller-Holst, O. Gorseth, S. Kjelstrup, Transport and equilibrium properties of Nafion® membranes with H$^+$ and Na$^+$ ions, Journal of Electroanalytical Chemistry. 442 (1998) 137–145. https://doi.org/10.1016/S0022-0728(97)00499-3.

[41]   S. Goldstein, D. Meyerstein, G. Czapski, The Fenton reagents, Free Radical Biology and Medicine. 15 (1993) 435–445. https://doi.org/10.1016/0891-5849(93)90043-T.

[42]   F. Andolfatto, R. Durand, A. Michas, P. Millet, P. Stevens, Solid polymer electrolyte water electrolysis: electrocatalysis and long-term stability, International Journal of Hydrogen Energy. 19 (1994) 421–427. https://doi.org/10.1016/0360-3199(94)90018-3.

[43]   S. Cherevko, S. Geiger, O. Kasian, A. Mingers, K.J.J. Mayrhofer, Oxygen evolution activity and stability of iridium in acidic media. Part 1. - Metallic iridium, Journal of Electroanalytical Chemistry. 773 (2016) 69–78. https://doi.org/10.1016/j.jelechem.2016.04.033.

[44]   P. Millet, F. Andolfatto, R. Durand, Design and performance of a solid polymer electrolyte water electrolyzer, International Journal of Hydrogen Energy. 21 (1996) 87–93. https://doi.org/10.1016/0360-3199(95)00005-4.